

Sodium and proton diffusion MRI as biomarkers for early therapeutic response in subcutaneous tumors[☆]

Victor D. Schepkin^{a,*}, Thomas L. Chenevert^a, Kyle Kuszpit^a, Kuei C. Lee^a, Charles R. Meyer^a, Timothy D. Johnson^b, Alnawaz Rehemtulla^a, Brian D. Ross^a

^aDepartment of Radiology, Center for Molecular Imaging, University of Michigan Medical School, Ann Arbor, MI 48109-0503, USA

^bDepartment of Biostatistics, Center for Molecular Imaging, University of Michigan Medical School, Ann Arbor, MI 48109-0503, USA

Received 16 October 2005; accepted 11 December 2005

Abstract

The ability to quantitate early effects of tumor therapeutic response using noninvasive imaging would have a major impact in clinical oncology. One area of active research interest is the ability to use MR techniques to detect subtle changes in tumor cellular density. In this study, sodium and proton diffusion MRI were compared for their ability to detect early cellular changes in tumors treated with a cytotoxic chemotherapy. Subcutaneous 9L gliosarcomas were treated with a single dose of 1,3-bis(2-chloroethyl)-1-nitrosourea. Both sodium and diffusion imaging modalities were able to detect changes in tumor cellularity as early as 2 days after treatment, which continued to evolve as increased signal intensities reached a maximum ~8 days posttreatment. Early changes in tumor sodium and apparent diffusion coefficient values were predictive of subsequent tumor shrinkage, which occurred ~10 days later.

Overall, therapeutical induced changes in sodium and diffusion values were found to have similar dynamic and spatial changes. These findings suggest that these imaging modalities detected similar early cellular changes after treatment. The results of this study support the continued clinical testing of diffusion MRI for evaluation of early tumor treatment response and demonstrate the complementary insights of sodium MRI for oncology applications.

© 2006 Elsevier Inc. All rights reserved.

Keywords: Oncology; Proton diffusion; Sodium; Magnetic resonance; Tumor; Chemotherapy

1. Introduction

Currently, there is significant interest in identifying biomarkers that are able to predict if a tumor will be responsive to a specific therapy before treatment using genomics/proteomics and during the course of treatment using imaging. Noninvasive imaging modalities have been increasingly investigated for their ability to provide early prediction of cancer treatment outcome. Because cellular changes can occur well in advance of tumor shrinkage [1–4], imaging approaches that are sensitive to cell viability

could provide a unique window of opportunity allowing for the early prediction of treatment outcome.

Changes in tumor water apparent diffusion coefficients (ADCs) [1–4] and sodium content are attracting increasing interest due to both preclinical and clinical success and from developments in high-magnetic-field technology [5–27]. In this study, the subcutaneous 9L tumor model was used to evaluate Na MRI for detection of early chemotherapeutic changes as compared with diffusion MRI. Both imaging modalities were performed simultaneously over a 3-week period after a single dose of chemotherapy. We found excellent correlation between tumor tissue sodium content (TSC) and ADC values demonstrating the ability of both modalities to detect treatment-induced changes in tumor cell membrane integrity. The results of this study support the hypothesis that the correlation between chemotherapy-induced changes in ADC values and sodium levels using MRI is reflective of their sensitivity to changes in the intra/extracellular space, an inherent link with overall cell membrane integrity. However,

[☆] Conflict of interest statement: T.L.C., A.R., and B.D.R. have a financial interest in the underlying technology (patent no. 6,567,684) discussed in this article. Furthermore, this technology is licensed to Molecular Therapeutics, Inc. in which A.R. and B.D.R. have a financial interest.

* Corresponding author. Department of Radiology, Center for Molecular Imaging, University of Michigan Medical School, Ann Arbor, MI 48109-0503, USA. Tel.: +1 734 763 5445; fax: +1 734 763 5447.

E-mail address: vschepki@umich.edu (V.D. Schepkin).

both modalities do not necessarily always convey the same information for a given voxel as they provide independent measures of tumor microenvironment. During successful interventions, as observed during chemotherapy, tumor cell destruction occurs relatively quickly, initiating coherent changes in both TSC and ADC values. The early increases in ADC and TSC observed well before any volumetric decrease provide compelling evidence that these noninvasive imaging modalities can be used as predictive biomarkers of cancer therapeutic efficacy.

2. Materials and methods

2.1. Cell culture

Rat 9L gliosarcoma cells (Passage 12) from the Brain Tumor Research Center at the University of California at San Francisco were maintained and grown as monolayer cultures in Dulbecco's modified Eagle's medium (DMEM) supplemented with 10% (vol/vol) heat-inactivated fetal bovine serum, 100 IU/ml penicillin and 100 μ g/ml streptomycin at 37 °C in a normally humidified atmosphere containing 95%/5% air/CO₂ mixture. Before implantation, cells were grown to confluence in a 175-cm² flask, harvested using a 0.25% trypsin/0.1% EDTA solution and counted. Cells were pelleted (800 \times g, 5 min), resuspended in serum-free DMEM at a concentration of \sim 10⁴ cells/ μ l and kept on ice until use. The 9L cells were carried only until Passage 40, at which time cells were reactivated from frozen stocks. Cell culture reagents were obtained from Invitrogen Life Technologies (Carlsbad, CA, USA).

2.2. Tumor implantation of animals

Male Fisher 344 rats weighing \sim 75 g were obtained from Harlan (Indianapolis, IN, USA). Animals ($N=12$) were anesthetized by intraperitoneal injection using an 87%/13% (vol/vol) ketamine/xylazine mixture. Under aseptic conditions, the rats were injected subcutaneously in the right hindquarter (where the top of the leg and the body meet) with 50 μ l of 9L cells (\sim 10⁴ cells/ μ l).

2.3. Chemotherapeutic treatment

Thirteen days after the tumor implantation, the 12 tumor-bearing rats were divided into two groups: 7 rats for the treatment group and 5 for the control group. The rats' average tumor size at the time of treatment (13 days after tumor implantation) was \sim 300 μ l. The treated group received 1,3-bis(2-chloroethyl)-1-nitrosourea (BCNU) therapy. A standard 100-mg BCNU preparation (Bristol Lab) was dissolved in ethanol and subsequently in 100% saline solution according to the recommended procedure described in the instructions for preparation. Dissolved BCNU was immediately used for a single-dose intraperitoneal injection of 26.6 mg/kg. All animal experiments were conducted according to the protocols approved by the University of Michigan Committee on Use and Care of Animals.

2.4. MRI

Sodium and proton MRI were performed serially every 2–3 days on all animals until sacrifice, when the tumor reached a volume of \sim 2 cm³. Proton and sodium MR scans were performed using a 9.4-T Varian MR scanner (120-mm clear horizontal bore, Varian, Palo Alto, CA, USA) and a double-tuned volume radiofrequency (RF) coil with an internal diameter of 34 mm and a length of 65 mm (Doty Scientific, Columbia, SC, USA). Animal body temperature was maintained during MRI scans using a temperature-controlled circulating-water heating pad. Anesthesia was maintained using a 1.25% vol/vol isoflurane/air gas mixture.

2.4.1. Sodium MRI

The tumor region of each rat was placed at the center of the RF coil. The axial length of the RF homogenous region (\pm 5%) was \sim 20 mm, which was sufficient to encompass the spatial extent of the tumors and to allow quantitative tumor sodium imaging. Because sodium has short T2 relaxation time components, a three-dimensional (3D) back-projection pulse sequence was used. In the original spin-echo 3D back-projection pulse sequence (Varian), two hard pulses were providing an echo time of 1000 μ s. The other parameters were as follows: readout gradient 1.3 G/cm; field of view (FOV) 64 \times 64 \times 64 mm; sodium signal was acquired with 64 complex points in readout direction using 32 \times 32 projections; TR=0.1 s; and scan time=28 min. Duration of the 90° pulse was 50 μ s. Sodium T1 relaxation time in normal rat muscle in our experiments was 37 \pm 1 ms at 9.4 T, thus yielding an almost unsaturated Na signal during 3D imaging. Back-projection reconstruction was performed using Matlab (V.7.0.1). Data were zero filled to 256 points before Fourier transform. The final output image matrix had 180 \times 180 \times 180 voxels for the sodium signal through the FOV.

Sodium tumor concentration was determined as an average for all voxels over the 3D volume of the tumor.

2.4.2. Proton MRI

The protocol for proton multislice diffusion MRI utilized an FOV of 40 \times 40 mm, an acquisition matrix of 128 \times 128, 15 slices, slice thickness of 1.5 mm, slice gap of 0.5 mm, TR of 3 s and TE of 40 ms. The diffusion spin-echo pulse sequence employed isotropic diffusion weighting by orthogonalization of x -, y - and z -gradient waveforms [28]. Specifically, the imaging plus diffusion gradient waveforms were designed to equalize diagonal elements and zero out off-diagonal elements of the b matrix. In addition, this sequence included first-order motion compensation and a 32-point navigator echo for phase correction before two-dimensional Fourier transform image reconstruction. Diffusion-weighted images (DWIs) at two b -factor settings were acquired for calculation of ADC maps: high b ($b=1082$ s/mm²) and low b ($b=117$ s/mm²). Proton images and ADC maps were reconstructed in Matlab, and

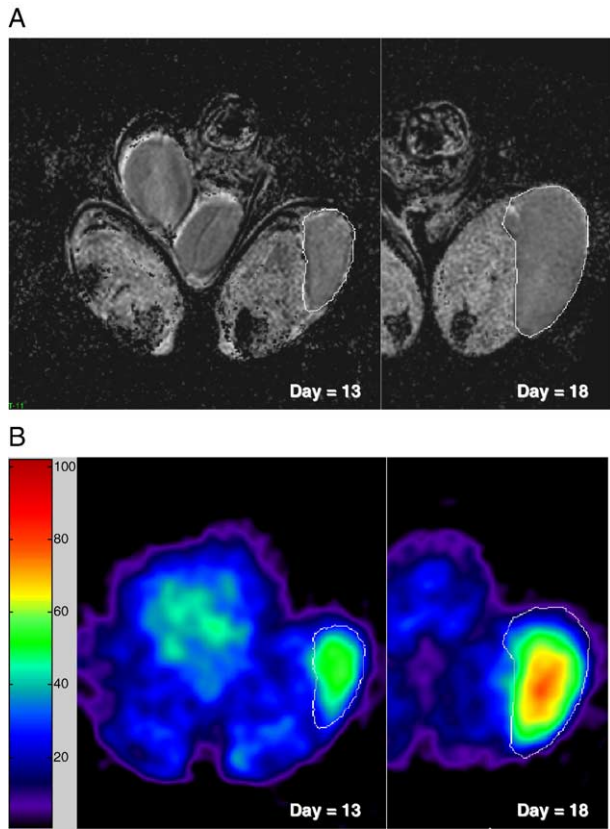


Fig. 1. Quantitative proton ADC maps (A) and corresponding coregistered sodium images (B) of a representative untreated tumor on Days 13 and 18 after tumor implantation. Tumor growth shown on the images (see right flank) does not produce any change in tumor diffusion. At the same time, tumor sodium concentration slightly increased, demonstrating the ability of Na to detect subtle changes in tumors.

the tumor volume and average ADC values were determined over a 3D volume of interest (VOI) for each temporal measurement.

2.5. Quantification and analysis

Three-dimensional sodium images were coregistered to the target proton multislice DWI and ADC image set. Use of a double-tuned coil dramatically minimized the coregistration procedure. This process placed all images onto a common geometrical frame, allowing the tumor VOI definition to be performed on available higher-quality images that were registered to the quantitative images of interest (i.e., sodium and ADC).

For quantification of sodium measurements, Na MR signals were compared with several reference samples consisting of saline at 38, 77 and 154 mM. The size of these reference samples was adjusted to fill the working volume of the coil. The difference in RF coil loading between animals and reference samples was corrected by adjusting the sodium tumor signals with a reverse ratio of the corresponding sodium 90° pulse durations.

Each animal had Na MRI and ADC measurements performed in axial planes through the tumor and in the

contralateral flank. Reproducibility of the imaging experimental conditions was assessed by stability of Na and ADC measurements in the contralateral region. The results of all ADC values and sodium concentrations are presented as average \pm S.E.M.

3. Results

BCNU treatment of subcutaneous 9L tumors was monitored over time using diffusion and sodium MRI. A representative example of a diffusion map from an untreated 9L tumor is shown in Fig. 1A. Although some heterogeneity is observed, overall, the ADC maps reveal a lower diffusion value relative to the host muscle tissue. In contrast, the sodium levels of the tumor were well above the normal muscle tissue and increased somewhat over time as shown in Fig. 1B. For example, on Day 18 after tumor implantation, sodium images revealed increases in tumor sodium concentration (Fig. 1B) whereas diffusion values remained consistent. Diffusion maps of tumors with BCNU revealed a significant increase in ADC values on Day 8, which returned to pretreatment levels by Day 17 (Fig. 2A).

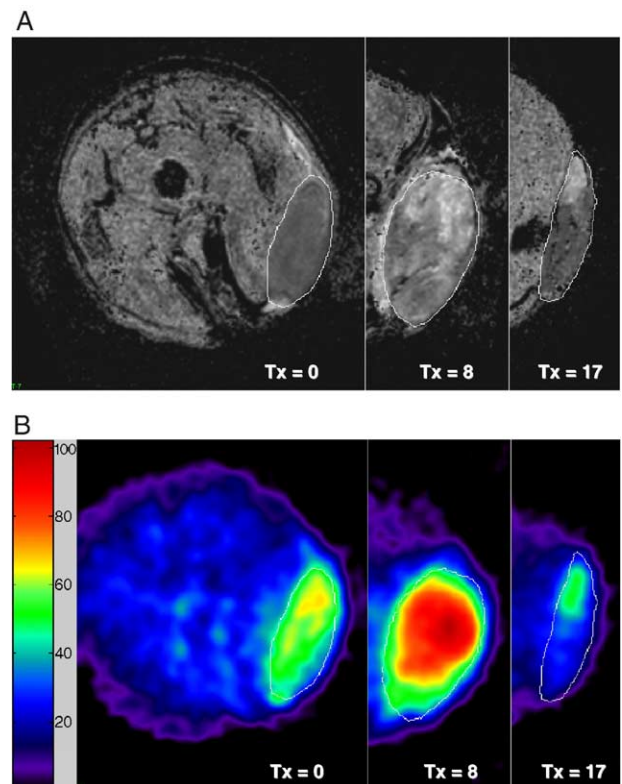


Fig. 2. Quantitative proton ADC maps (A) and corresponding coregistered sodium MR images (B) of treated tumors on Days 0, 8 and 17 after a single dose of BCNU. Heterogeneous tumor ADC increases along with intensive sodium uptake can be seen on Day 8 posttreatment. On Day 17, tumor ADC values and sodium concentration are returning to their pretreatment values. Repopulation of the tumor mass can be seen on Day 17 as a gray (low diffusion) region of the tumor on the ADC map (A), which corresponds to the low Na concentration in the sodium image (B).

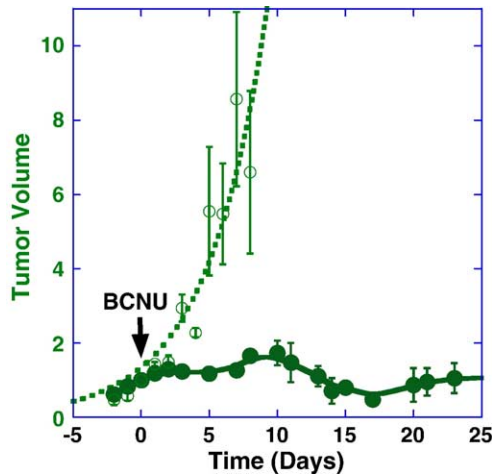


Fig. 3. The time course of 9L tumor growth in BCNU-treated (●) and BCNU-untreated rodents (○). Tumor volumes were normalized to 1 at the time of treatment, denoted by the downward pointing arrow on Day 0.

Changes in tumor sodium content paralleled the changes observed in the ADC maps as shown in Fig. 2B.

A comparison of the tumor volumes for control versus treated tumors is provided in Fig. 3. These data reveal that treatment with BCNU significantly inhibited the growth of the subcutaneous 9L tumor in the treated group versus the untreated group. In fact, tumor volume in untreated 9L tumors during the experiment increased eightfold (Fig. 3), with a volumetric doubling time of 3.0 ± 0.5 days.

Three days after treatment with BCNU, the average rate of ADC increase was $\sim 0.15 \times 10^{-3} \text{ mm}^2/\text{s}/\text{day}$ (Fig. 4). Thereafter, mean ADC reached a maximum of $(1.87 \pm 0.06) \times 10^{-3} \text{ mm}^2/\text{s}$ on Day 8 posttreatment. The mean ADC values in untreated tumors remained constant over time at $(1.07 \pm 0.02) \times 10^{-3} \text{ mm}^2/\text{s}$, with no significant change over

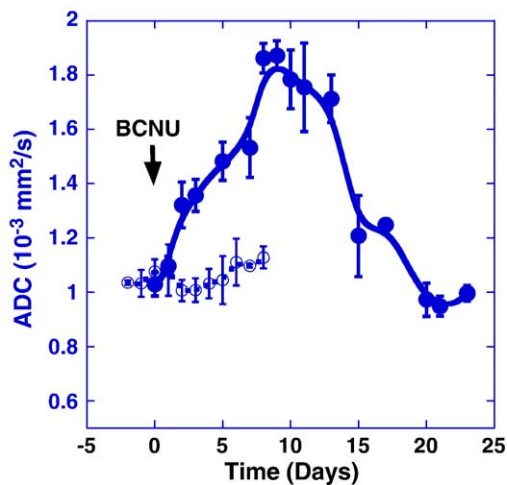


Fig. 4. The time course of subcutaneous tumor ADCs in BCNU-treated (●) and BCNU-untreated rodents (○). Time 0 corresponds to administration of BCNU 13 days after tumor implantation. Note the large increase in tumor ADC values observed for the treated group relative to the untreated group of tumors.

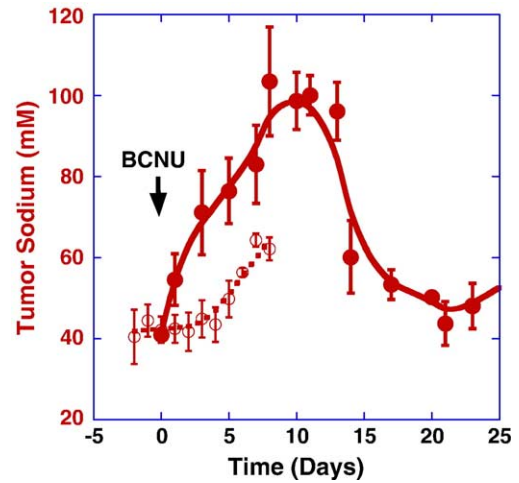


Fig. 5. The time course of tumor sodium concentration in BCNU-treated (●) and BCNU-untreated rodents (○). Time 0 corresponds to the time of BCNU injection (13 days after tumor implantation). Tumor sodium concentration in untreated animals slowly increases at the later stages of tumor growth.

time as shown in Fig. 4. For comparison, the ADC values in a contralateral normal flank tissue were $(1.29 \pm 0.02) \times 10^{-3} \text{ mm}^2/\text{s}$.

The dynamic changes in tumor ADC and TSC after BCNU treatment demonstrate quantitatively a very close similarity in therapy response detected by these imaging modalities (Figs. 4 and 5). The initial rate of tumor sodium increase after BCNU injection was $\sim 5.6 \text{ mM}/\text{day}$. The average tumor sodium concentration reached a maximum of $\sim 100 \text{ mM}$ on Day 8 after initiation of therapy. The initial tumor Na concentration in nontreated tumors was $42 \pm 2 \text{ mM}$ (Fig. 5). It is important to note that during 9 days of observation, tumor sodium in nontreated tumors also increased over time, as the tumor volume increased eightfold. For comparison, the Na concentration in a

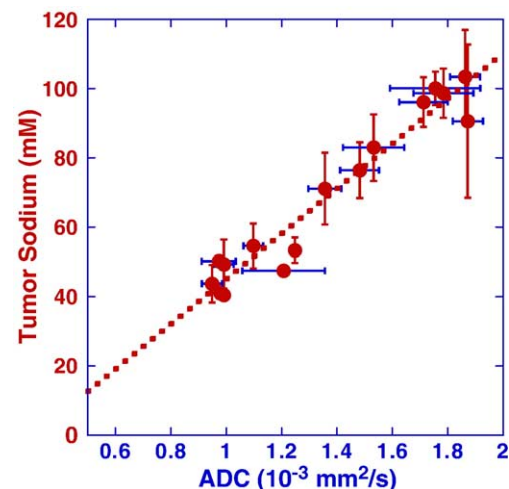


Fig. 6. A plot of the average tumor sodium concentration versus average tumor ADC values obtained after tumor treatment ($y = -19.9 + 65.1 \times 10^3 \times \text{ADC}$; $R = .97$).

contralateral normal flank tissue was $\sim 20 \pm 2$ mM, which is much less than that in tumor.

It was noted that, during tumor shrinkage, tumor ADC and sodium concentration were still elevated above pre-BCNU levels. Both sodium and ADC reached their pretreatment values on approximately Day 18 of posttreatment, which corresponded to the maximum regression of the tumor volume.

Comparison of changes in proton ADC values and sodium concentrations in subcutaneous tumors after therapy revealed an excellent correlation (Fig. 6). The relationship between the two modalities was fitted by the equation $[\text{Na}] \text{ mM} = -19.9 + 65.1 \times 10^3 \times \text{ADC}$, with a correlation coefficient (R) of .97. The total range of changes in tumor sodium concentration after therapy was from ~ 40 mM (Day 0) to 100 mM (Day 8), whereas total changes in diffusion were from $1 \times 10^{-3} \text{ mm}^2/\text{s}$ (Day 0) to $1.9 \times 10^{-3} \text{ mm}^2/\text{s}$ (Day 8).

4. Discussion

This study presents evidence for the correlation of changes in TSC with those in ADC values during chemotherapy. The correspondence of temporal changes observed between sodium and ADC images for this tumor and, ultimately, their well-defined linear dependence (Fig. 4) support the hypothesis that this correlation could be a general phenomenon and that both modalities represent altered tumor cellularity during cancer treatment.

It is expected that sodium and ADCs have a similar capacity to reflect changes in cellularity during interventions. All functioning cells have a large transmembrane gradient of Na, with a low intracellular concentration ($\text{Na}_{\text{in}} \sim 15$ mM) and a high extracellular concentration ($\text{Na}_{\text{ex}} \sim 140$ mM). Because of the limited extracellular space in muscle, the average tissue Na concentration is ~ 20 – 30 mM, as can be derived from the data for intracellular Na in rat muscle [29]. Thus, disruption of the Na transmembrane gradient, as a result of interventions, could initiate a dramatic increase in tissue sodium to a maximum concentration up to the value found in extracellular space (~ 140 mM). A similar situation could occur for ADC, where loss of membrane function integrity leads to increased volume of extracellular space; thus, water mobility becomes less restricted and is reflected in tumor ADC values. If these cellular processes are initiated by tumor therapy, it is reasonable to assume that the corresponding changes in sodium and ADC values should have a temporal correlation. Our study demonstrated that both imaging modalities were capable of detecting dynamic therapeutically induced changes in tumors. This conclusion is also supported by recent MRI experiments on RIF-1 tumors treatment by cyclophosphamide [21].

Data presented in this current work reveal that changes in Na and ADC tumor values after BCNU therapy could be detected 2–3 days after initiation of treatment, revealing that

these measurements can serve as early therapeutic outcome biomarkers. In fact, treatment initiated a rapid rise in tumor sodium increase of ~ 5.6 mM/day among the treated animals, as compared with the untreated animals that had an average rate of ~ 2.7 mM/day. An increase of tumor sodium eventually could lead to a burst of tumor cells, detectable as an increase in a tumor's ADC and Na at the same time, which is a sign of the latest stages of cell death. In this regard, sodium MRI may deliver grading and prognostic information about tumors comparable with those of nuclear imaging methods [30].

5. Conclusion

This study demonstrates that, using an animal model, there is an excellent correlation between tumor sodium and ADC during chemotherapy. The experiments support the hypothesis that this correlation could be a general phenomenon relevant for other tumors in other anatomical sites. The study reveals the ability of sodium MRI to perform the same diagnostic and predictive role during cancer therapy as does ADC mapping. Low sodium signal intensities have certain limitations on the resolution of sodium MRI. However, sodium images on 3- to 4-T MR scanners are already a reality. An advantage of sodium MRI is that it has less intensive susceptibility artifact, which is a valuable feature for any surface tumor and could provide a more robust quantitative approach in areas where cardiac or respiratory motion is a significant issue.

The results of this study support the current clinical trials of ADC as an indicator of tumor cellularity during cancer therapy and demonstrate the complementary possibility of using Na MRI. The future development of high-field scanners will further aid in facilitating the utilization of sodium MRI in clinical oncology.

Acknowledgments

This study was supported by a John and Suzanne Munn Endowment research grant, a Michigan Comprehensive Cancer Center grant and a National Institutes of Health grant (P01CA85878, P50CA93990 and R24CA83099).

We thank Mukilan Muthuswami for implementing the experimental protocol and Daniel Hall, Ben Hoff and Dr. Bradford Moffat for their valuable help and discussion.

References

- [1] Ross BD, Moffat BA, Lawrence TS, Mukherji SK, Gebarski SS, Quint DJ, et al. Evaluation of cancer therapy using diffusion magnetic resonance imaging. *Mol Cancer Ther* 2003;2(6):581–7.
- [2] Chenevert TL, Meyer CR, Moffat BA, Rehemtulla A, Mukherji SK, Gebarski SS, et al. Diffusion MRI: a new strategy for assessment of cancer therapeutic efficacy. *Mol Imaging* 2002;1(4):336–43.
- [3] Schepkin VD, Ross BD, Chenevert TL, Rehemtulla A, Sharma S, Kumar M, et al. Sodium magnetic resonance imaging of

- chemotherapeutic response in a rat glioma. *Magn Reson Med* 2005;53(1):85–92.
- [4] Moffat BA, Chenevert TL, Lawrence TS, Meyer CR, Johnson TD, Dong Q, et al. Functional diffusion map: a noninvasive MRI biomarker for early stratification of clinical brain tumor response. *Proc Natl Acad Sci U S A* 2005;102(15):5524–9.
- [5] Bartha R, Lee TY, Hogan MJ, Hughes S, Barberi E, Rajakumar N, et al. Sodium T2*-weighted MR imaging of acute focal cerebral ischemia in rabbits. *Magn Reson Imaging* 2004;22(7):983–91.
- [6] Boada FE, Shen GX, Chang SY, Thulborn KR. Spectrally weighted twisted projection imaging: reducing T2 signal attenuation effects in fast three-dimensional sodium imaging. *Magn Reson Med* 1997;38(6):1022–8.
- [7] Borthakur A, Shapiro EM, Akella SV, Gougoutas A, Kneeland JB, Reddy R. Quantifying sodium in the human wrist in vivo by using MR imaging. *Radiology* 2002;224(2):598–602.
- [8] Clayton DB, Lenkinski RE. MR imaging of sodium in the human brain with a fast three-dimensional gradient-recalled-echo sequence at 4 T. *Acad Radiol* 2003;10(4):358–65.
- [9] Constantinides CD, Gillen JS, Boada FE, Pomper MG, Bottomley PA. Human skeletal muscle: sodium MR imaging and quantification — potential applications in exercise and disease. *Radiology* 2000;216(2):559–68.
- [10] Jerecic R, Bock M, Nielles-Vallespin S, Wacker C, Bauer W, Schad LR. ECG-gated ²³Na-MRI of the human heart using a 3D-radial projection technique with ultra-short echo times. *MAGMA* 2004;16(6):297–302.
- [11] Kohler S, Preibisch C, Nittka M, Haase A. Fast three-dimensional sodium imaging of human brain. *MAGMA* 2001;13(2):63–9.
- [12] Steidle G, Graf H, Schick F. Sodium 3-D MRI of the human torso using a volume coil. *Magn Reson Imaging* 2004;22(2):171–80.
- [13] Goodman JA, Kroenke CD, Bretthorst GL, Ackerman JJ, Neil JJ. Sodium ion apparent diffusion coefficient in living rat brain. *Magn Reson Med* 2005;53(5):1040–5.
- [14] Wheaton AJ, Borthakur A, Dodge GR, Kneeland JB, Schumacher HR, Reddy R. Sodium magnetic resonance imaging of proteoglycan depletion in an in vivo model of osteoarthritis. *Acad Radiol* 2004;11(1):21–8.
- [15] Greiser A, Haase A, von Kienlin M. Improved cardiac sodium MR imaging by density-weighted phase-encoding. *J Magn Reson Imaging* 2005;21(1):78–81.
- [16] Maril N, Margalit R, Mispelner J, Degani H. Sodium magnetic resonance imaging of diuresis: spatial and kinetic response. *Magn Reson Med* 2005;53(3):545–52.
- [17] Bansal N, Germann MJ, Lazar I, Malloy CR, Sherry AD. In vivo Na-23 MR imaging and spectroscopy of rat brain during TmDOTP5-infusion. *J Magn Reson Imaging* 1992;2(4):385–91.
- [18] Ouwerkerk R, Bleich KB, Gillen JS, Pomper MG, Bottomley PA. Tissue sodium concentration in human brain tumors as measured with ²³Na MR imaging. *Radiology* 2003;227(2):529–37.
- [19] Thulborn KR, Davis D, Adams H, Gindin T, Zhou J. Quantitative tissue sodium concentration mapping of the growth of focal cerebral tumors with sodium magnetic resonance imaging. *Magn Reson Med* 1999;41(2):351–9.
- [20] Winter PM, Poptani H, Bansal N. Effects of chemotherapy by 1,3-bis(2-chloroethyl)-1-nitrosourea on single-quantum- and triple-quantum-filtered ²³Na and ³¹P nuclear magnetic resonance of the subcutaneously implanted 9L glioma. *Cancer Res* 2001;61(5):2002–7.
- [21] Babsky AM, Hekmatyar SK, Zhang H, Solomon JL, Bansal N. Application of ²³Na MRI to monitor chemotherapeutic response in RIF-1 tumors. *Neoplasia* 2005;7(7):658–66.
- [22] Kline RP, Wu EX, Petrylak DP, Szabolcs M, Alderson PO, Weisfeldt ML, et al. Rapid in vivo monitoring of chemotherapeutic response using weighted sodium magnetic resonance imaging. *Clin Cancer Res* 2000;6(6):2146–56.
- [23] Boada FE, Davis D, Walter K, Torres-Trejo A, Kondziolka D, Bartynski W, et al. Single and triple quantum sodium MRI of primary human brain tumors. Toronto, Canada; 2003. p. 525.
- [24] Bartha R, McNab J, Rajakumar C, Megyesi J, Watling C. 4 Tesla ¹H MR spectroscopy and ²³Na imaging in low grade glioma. Miami, Florida, USA; 2005. p. 668.
- [25] Sharma R, Kline RP, Wu EX, Katz JK. Rapid in vivo Taxotere quantitative chemosensitivity response by 4.23 Tesla sodium MRI and histo-immunostaining features in *N*-methyl-*N*-nitrosourea induced breast tumors in rats. *Cancer Cell Int* 2005;5(1):26.
- [26] Kaplan O, Kushnir T, Askenazy N, Knubovets T, Navon G. Role of nuclear magnetic resonance spectroscopy (MRS) in cancer diagnosis and treatment: ³¹P, ²³Na, and ¹H MRS studies of three models of pancreatic cancer. *Cancer Res* 1997;57(8):1452–9.
- [27] Jacobs MA, Ouwerkerk R, Wolff AC, Stearns V, Bottomley PA, Barker PB, et al. Multiparametric and multinuclear magnetic resonance imaging of human breast cancer: current applications. *Technol Cancer Res Treat* 2004;3(6):543–50.
- [28] Moffat BA, Hall DE, Stojanovska J, McConville PJ, Moody JB, Chenevert TL, et al. Diffusion imaging for evaluation of tumor therapies in preclinical animal models. *MAGMA* 2004;17(3–6):249–59.
- [29] Lindinger MI, Heigenhauser GJ. Intracellular ion content of skeletal muscle measured by instrumental neutron activation analysis. *J Appl Physiol* 1987;63(1):426–33.
- [30] Benard F, Romsa J, Hustinx R. Imaging gliomas with positron emission tomography and single-photon emission computed tomography. *Semin Nucl Med* 2003;33(2):148–62.